HEFAT2010
7th International Conference on Heat Transfer, Fluid Mechanics and Thermodynamics
19-21 July 2010
Antalya, Turkey

A MATHEMATICAL SIMULATION OF DOUBLE-DIFFUSIVE CONJUGATE NATURAL CONVECTION IN AN ENCLOSURE

Kuznetsov G.V.[a] and Sheremet M.A.*[,b]
*Author for correspondence
[a] Faculty of Thermal Power Engineering
Tomsk Polytechnic University, Tomsk, 634050, Russia
[b] Faculty of Mechanics and Mathematics
Tomsk State University, Tomsk, 634050, Russia
E-mail: Michael-sher@yandex.ru

ABSTRACT

Transient thermosolutal convection in a cubical enclosure having finite thickness walls filled with air, submitted to temperature and concentration gradients, is studied numerically. In the first series of numerical simulations, the influence of Rayleigh number on fluid motion and heat and mass transfer $\left(Br=1,\ Ra=10^4-10^5\right)$ is analyzed. The second series deals with the effect of the dimensionless time $\left(Br=1,\ Ra=5\cdot10^4,\ \tau=1-100\right)$. In the third series the influence of the conductivity ratio on heat and mass transfer $\left(Br=1,\ Ra=10^5,\ k_{fs}=0.037,\ 0.0037\right)$ on heat and mass transfer is investigated. Comprehensive Nusselt and Sherwood numbers data are presented as functions of the governing parameters mentioned above.

INTRODUCTION

Natural convection heat and mass transfer in enclosures has numerous industrial and geophysical applications, such as petrochemical process, fuel cells, pollutant dispersions in soil and underground water, design of heat exchangers, channel type solar energy collectors, and thermo-protection systems. Therefore, the characteristics of natural convection heat and mass transfer are relatively important. Convection flows driven by temperature and concentration differences is studied extensively [1–8]. Sezai and Mohamad [1], presented results for three-dimensional flow in a cubic cavity filled with porous medium and subjected to opposing thermal and concentration gradients. Mohamad and Bennacer [2] numerically analyzed three-dimensional flow in an enclosure heated differently and stably stratified in imposed vertically. Their results revealed that the difference between two- and three-dimensional models is not that significant as far as heat and mass transfer is concerned. Jer-Huan Jang et al. [3] numerically examined the natural convection heat and mass transfer along a vertical wavy surface by using Prandtl's transposition theorem and investigated the effect of irregular surfaces on the characteristics of natural convection heat and mass transfer. It was found that increasing Schmidt number the skin-friction coefficient and local Nusselt number decrease but local Sherwood number increases. Chourasia and Goswami [4] numerically simulated the three-dimensional transport phenomena in heat and mass generating porous medium cooled under natural convective environment. They found that CFD is a useful tool for obtaining accurate solutions of engineering problems such as modelling the transport phenomena in partially permeable packages. Chakraborty and Dutta [5] used a three-dimensional transient mathematical model to study the interaction of double-diffusive natural convection and non-equilibrium solidification of a binary mixture in a cubic enclosure cooled from a side. It was found that the three-dimensional transport leads to a global macrosegregation resulting in composition variations across the longitudinal planes, which cannot be captured by two-dimensional mathematical models. Papanicolaou and Belessiotis [6] numerically studied the double-diffusive natural convection in an asymmetric trapezoidal enclosure with vertical temperature and concentration gradients. Fu-Yun Zhao et al. [7] investigated the double-diffusive convective flow of a binary mixture in a porous enclosure subject to localized heating and salting from one side. The physical model for the momentum conservation equation makes use of the Darcy-Brinkman equation, which allows the non-slip boundary condition on a solid wall to be satisfied. It was found that overall heat and mass transfer rates tend to be minimized in the transitional range to the point of flow reversal for any segment location. Alloui et al. [8] used the Darcy model with the Boussinesq approximation to study natural convection in a porous medium saturated by a binary fluid. It was found that both unicellular and bicellular symmetrical circulations are possible for centrally located heated element.

NOMENCLATURE

$Bi = hL/k$	[-]	Biot number
$Br = \frac{\beta_C (C_{cs} - C_0)}{\beta_T (T_{hs} - T_0)}$	[-]	buoyancy ratio
C	[-]	concentration of pollutant
C_{cs}	[-]	contaminant source concentration
C_0	[-]	initial concentration
D	[m^2/s]	mass diffusivity
g	[m/s^2]	gravitational acceleration
h	[W/m^{2}K]	heat transfer coefficient
k	[W/mK]	thermal conductivity
$k_{fs} = k_f/k_s$	[-]	thermal conductivity ratio
L	[m]	length of the gas cavity
Nu	[-]	Nusselt number
$Pr = \nu/\alpha$	[-]	Prandtl number
$Ra = \frac{g\beta_I (T_{hs} - T_0) L^3}{\nu\alpha}$	[-]	Rayleigh number
$Sc = \nu/D$	[-]	Schmidt number
Sh	[-]	Sherwood number
$Sk = \varepsilon\sigma L (T_{hs} - T_0)^3 / k$	[-]	Stark number
T	[K]	temperature
T_{hs}	[K]	heat source temperature
T_0	[K]	initial temperature
U, V, W	[-]	dimensionless velocity components in X, Y, Z directions
x, y, z	[m]	Cartesian coordinates
X, Y, Z	[-]	dimensionless Cartesian coordinates
Greek symbols		
α	[m^2/s]	thermal diffusivity
$\alpha_{sf} = \alpha_s/\alpha_f$	[-]	thermal diffusivity ratio
β_C	[-]	coefficient of volumetric expansion due to concentration change
β_T	[K^{-1}]	coefficient of volumetric expansion due to temperature change
ε	[-]	specific emissitivity factor
$\zeta_e = T_e/(T_{hs} - T_0)$	[-]	temperature parameter
$\zeta_0 = T_0/(T_{hs} - T_0)$	[-]	temperature parameter
Θ	[-]	dimensionless temperature
ν	[m^2/s]	kinematic viscosity
ξ	[-]	dimensionless concentration
σ	[W/m^{2}K^4]	Stephen-Boltzman constant
τ	[-]	dimensionless time
Ψ_x, Ψ_y, Ψ_z	[-]	dimensionless vector potential functions
$\Omega_x, \Omega_y, \Omega_z$	[-]	dimensionless components of vorticity vector
Subscripts		
cs		contaminant source
e		environment
f		fluid
hs		heat source
s		solid
0		initial

Most of the previous studies about enclosures aren't concerned with the three-dimensional cavity having finite thickness walls in conditions of convective-radiative heat exchange with an environment. Conjugate natural convection heat and mass transfer in Newtonian fluid in three-dimensional enclosure having finite thickness walls has not been well investigated. The objective of this study is to examine numerically the three-dimensional transient double-diffusive natural convection in an enclosure having finite thickness walls.

MATHEMATICAL MODEL

In this investigation, it is assumed that the domain of interest (Figure 1) is a three-dimensional enclosure bounded by solid walls with a finite thickness and conductivity. The heat and mass sources located at the bottom of the cavity are kept at constant temperature and concentration respectively. The convective-radiative heat exchange with an environment is modeled on one of the external sides (x = 0). Other external sides are assumed to be adiabatic and impermeable. It is assumed in the analysis that the thermophysical properties of the solid walls and of the fluid are independent of temperature, and the flow is laminar. The fluid is Newtonian, viscous, heat-conducting, and the Boussinesq approximation is valid. The fluid motion and heat and mass transfer in the cavity are assumed to be three-dimensional. The interactions between heat and mass exchanges known under the name of Soret and Dufour effects are supposed to be negligible. The viscous dissipation is negligible too.

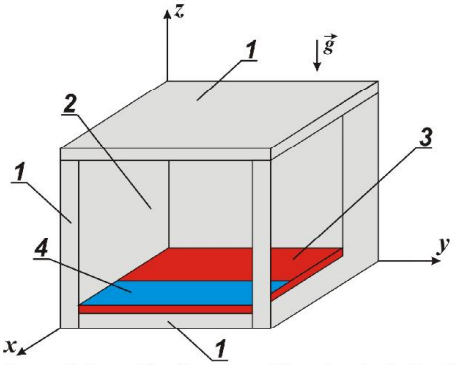

Figure 1 Schematic diagram of the physical situation: *1* – walls; *2* – gas; *3* – heat source; *4* – contaminant source

Based on the above-mentioned assumptions, the governing equations in the dimensionless variables such as vector potential functions, vorticity vector and temperature [9-11] for the fluid can be written as follows:

$$\frac{\partial \Omega_x}{\partial \tau} + U\frac{\partial \Omega_x}{\partial X} + V\frac{\partial \Omega_x}{\partial Y} + W\frac{\partial \Omega_x}{\partial Z} - \Omega_x\frac{\partial U}{\partial X} - \Omega_y\frac{\partial U}{\partial Y} - \Omega_z\frac{\partial U}{\partial Z} = \sqrt{\frac{Pr}{Ra}}\left(\frac{\partial^2 \Omega_x}{\partial X^2} + \frac{\partial^2 \Omega_x}{\partial Y^2} + \frac{\partial^2 \Omega_x}{\partial Z^2}\right) + \frac{\partial \Theta}{\partial Y} + Br\frac{\partial \xi}{\partial Y} \quad (1)$$

$$\frac{\partial \Omega_y}{\partial \tau} + U\frac{\partial \Omega_y}{\partial X} + V\frac{\partial \Omega_y}{\partial Y} + W\frac{\partial \Omega_y}{\partial Z} - \Omega_x\frac{\partial V}{\partial X} - \Omega_y\frac{\partial V}{\partial Y} - \Omega_z\frac{\partial V}{\partial Z} = \sqrt{\frac{Pr}{Ra}}\left(\frac{\partial^2 \Omega_y}{\partial X^2} + \frac{\partial^2 \Omega_y}{\partial Y^2} + \frac{\partial^2 \Omega_y}{\partial Z^2}\right) - \frac{\partial \Theta}{\partial X} - Br\frac{\partial \xi}{\partial X} \quad (2)$$

$$\frac{\partial \Omega_z}{\partial \tau}+U\frac{\partial \Omega_z}{\partial X}+V\frac{\partial \Omega_z}{\partial Y}+W\frac{\partial \Omega_z}{\partial Z}-\Omega_x\frac{\partial W}{\partial X}- \\ -\Omega_y\frac{\partial W}{\partial Y}-\Omega_z\frac{\partial W}{\partial Z}=\sqrt{\frac{Pr}{Ra}}\left(\frac{\partial^2\Omega_z}{\partial X^2}+\frac{\partial^2\Omega_z}{\partial Y^2}+\frac{\partial^2\Omega_z}{\partial Z^2}\right) \tag{3}$$

$$\frac{\partial^2\Psi_x}{\partial X^2}+\frac{\partial^2\Psi_x}{\partial Y^2}+\frac{\partial^2\Psi_x}{\partial Z^2}=-\Omega_x \tag{4}$$

$$\frac{\partial^2\Psi_y}{\partial X^2}+\frac{\partial^2\Psi_y}{\partial Y^2}+\frac{\partial^2\Psi_y}{\partial Z^2}=-\Omega_y \tag{5}$$

$$\frac{\partial^2\Psi_z}{\partial X^2}+\frac{\partial^2\Psi_z}{\partial Y^2}+\frac{\partial^2\Psi_z}{\partial Z^2}=-\Omega_z \tag{6}$$

$$\frac{\partial \Theta}{\partial \tau}+U\frac{\partial \Theta}{\partial X}+V\frac{\partial \Theta}{\partial Y}+W\frac{\partial \Theta}{\partial Z}= \\ =\frac{1}{\sqrt{Ra\cdot Pr}}\left(\frac{\partial^2\Theta}{\partial X^2}+\frac{\partial^2\Theta}{\partial Y^2}+\frac{\partial^2\Theta}{\partial Z^2}\right) \tag{7}$$

$$\frac{\partial \xi}{\partial \tau}+U\frac{\partial \xi}{\partial X}+V\frac{\partial \xi}{\partial Y}+W\frac{\partial \xi}{\partial Z}= \\ =\frac{1}{Sc}\sqrt{\frac{Pr}{Ra}}\left(\frac{\partial^2\xi}{\partial X^2}+\frac{\partial^2\xi}{\partial Y^2}+\frac{\partial^2\xi}{\partial Z^2}\right) \tag{8}$$

and energy equation for the solid walls can be written

$$\frac{\partial \Theta}{\partial \tau}=\frac{\alpha_{sf}}{\sqrt{Ra\cdot Pr}}\left(\frac{\partial^2\Theta}{\partial X^2}+\frac{\partial^2\Theta}{\partial Y^2}+\frac{\partial^2\Theta}{\partial Z^2}\right) \tag{9}$$

The dimensionless variables were obtained by using the characteristic scales L, $\sqrt{L/g\beta_T(T_{hs}-T_0)}$, $\sqrt{g\beta_T(T_{hs}-T_0)L}$, $(T_{hs}-T_0)$, $(C_{cs}-C_0)$, $\sqrt{g\beta_T(T_{hs}-T_0)/L}$, $\sqrt{g\beta_T(T_{hs}-T_0)L^3}$ corresponding to length, time, velocity, temperature, concentration, vorticity, and vector potential functions, respectively.

The initial and boundary conditions for the formulated problem (1)–(9) are as follows.

Initial conditions are

$$\Psi_x(X,Y,Z,0)=0,\quad \Omega_x(X,Y,Z,0)=0$$
$$\Psi_y(X,Y,Z,0)=0,\quad \Omega_y(X,Y,Z,0)=0$$
$$\Psi_z(X,Y,Z,0)=0,\quad \Omega_z(X,Y,Z,0)=0$$

$\Theta(X,Y,Z,0)=\xi(X,Y,Z,0)=0$, except temperature for heat source on which $\Theta=1$ and concentration for contaminant source where $\xi=1$ during the whole process time.

Boundary conditions are

- convective-radiative heat exchange with an environment is modeled at the wall $X=0$

$$\frac{\partial \Theta}{\partial X}=Bi(\Theta-\Theta_e)+Sk\cdot\left[(\Theta+\zeta_0)^4-\zeta_e^4\right]$$

- at the rest external walls for the equation (9) heat insulation conditions are set

$$\frac{\partial \Theta}{\partial X^i}=0 \qquad X^1\equiv X, X^2\equiv Y, X^3\equiv Z$$

- at the solid-fluid interfaces parallel to plane *XZ*:

$$\Psi_x=\frac{\partial \Psi_y}{\partial Y}=\Psi_z=\frac{\partial \xi}{\partial Y}=0 \quad \begin{cases}\Theta_s=\Theta_f \\ \dfrac{\partial \Theta_s}{\partial Y}=k_{fs}\dfrac{\partial \Theta_f}{\partial Y}\end{cases}$$

- at the solid-fluid interfaces parallel to plane *XY*:

$$\Psi_x=\Psi_y=\frac{\partial \Psi_z}{\partial Z}=\frac{\partial \xi}{\partial Z}=0 \quad \begin{cases}\Theta_s=\Theta_f \\ \dfrac{\partial \Theta_s}{\partial Z}=k_{fs}\dfrac{\partial \Theta_f}{\partial Z}\end{cases}$$

- at the solid-fluid interfaces parallel to plane *YZ*:

$$\frac{\partial \Psi_x}{\partial X}=\Psi_y=\Psi_z=\frac{\partial \xi}{\partial X}=0 \quad \begin{cases}\Theta_s=\Theta_f \\ \dfrac{\partial \Theta_s}{\partial X}=k_{fs}\dfrac{\partial \Theta_f}{\partial X}\end{cases}$$

Equations (1)–(9) with corresponding initial and boundary conditions have been solved by means of finite differences method [10-12].

The locally one-dimensional scheme of Samarskii [12] was used to solve energy equations (7) and (9), contaminant transport equation (8) and equations for the vorticity vector components (1)–(3). In this scheme, the solution to a three-dimensional problem reduces to sequential solution to the one-dimensional systems. The resulting set of discretized equations for each variable was solved by a line-by-line procedure, combining the tri-diagonal matrix algorithm (TDMA). An implicit difference scheme was used. Equations (4)–(6) were solved by a point successive over-relaxation method (PSOR) with an optimum relaxation factor. The mesh size is chosen on the basis of a compromise between running time and accuracy of the results.

Validation of Numerical Models

The accuracy of the program developed by the authors was checked by preparing the benchmark solutions both for non-conjugate and conjugate problems. In case of non-conjugate analysis, well-known benchmark of 3D natural convection in a differently heated cubical enclosure with adiabatic side walls [13, 14]. These benchmark results are shown in Table 1.

Table 1
Variations of average Nusselt number of heat wall with Rayleigh number (the first benchmark)

Ra	[13]	[14]	Present uniform grid	
			50×50×50	60×60×60
10^4	2.055	2.100	2.075	2.071
10^5	4.339	4.361	4.494	4.446
10^6	8.656	8.770	9.719	9.432

For conjugate problem benchmark solution has been obtained by using results [15]. Table 2 shows the good comparison between the results.

Table 3
Variations of average Nusselt number with Grashof number and heat conductivity ratio

Gr	k_{sf}	[15]	[16]	Present
10^3	1	0.87	0.877	0.872
	5	1.02		1.023
	10	1.04		1.046
10^5	1	2.08	2.082	2.116
	5	3.42		3.421
	10	3.72		3.781
10^6	1	2.87	2.843	3.002
	5	5.89		6.306
	10	6.81		6.935

It can be seen in Tables 1, 2 that the agreement is good, with a maximum deviation of 8% in the mean Nusselt number.

RESULTS AND DISCUSSION

Numerical analysis of the boundary value problem (1)–(9) has been carried out at following dimensionless complexes such as $10^4 \le Ra \le 10^5$, $Pr = 0.7$, $k_{fs} = 0.037,\ 0.0037$, $Br = 0,\ 1$ describing the basic modes of conjugate double-diffusive natural convection in enclosures. Our main attention was paid to the effect of the heat source strength (Ra), the contaminant source strength (Br), the dimensionless time and the thermal conductivity ratio on formation of the thermal modes and hydrodynamic structures in the domain of interest (Figure 1).

Velocity fields and isosurfaces of the vertical velocity component at $Br = 1$, $k_{fs} = 0.0037$, $\tau = 100$ and different values of the Rayleigh number are presented in Figure 2 and Figure 3.

The increase in the Rayleigh number (Figure 3) leads both to change of convective flow intensity in the gas cavity and to modification of the velocity field in the center of the domain of interest. Figure 3 shows appearance of the additional descending flows in the center which are caused both influence of heat and contaminant sources, and effect of an environment.

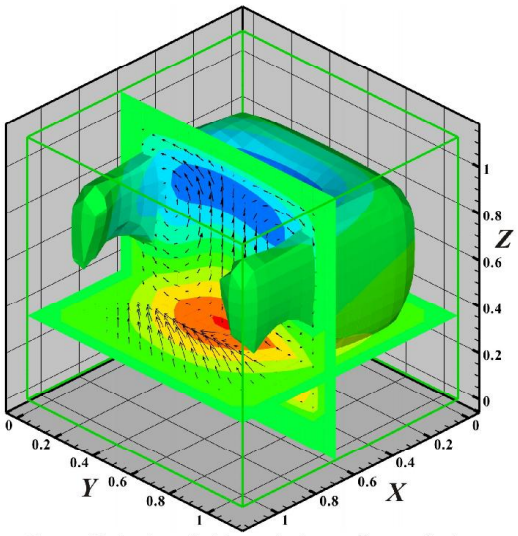

Figure 2 Velocity field and isosurface of the vertical velocity component at $Ra = 10^4$

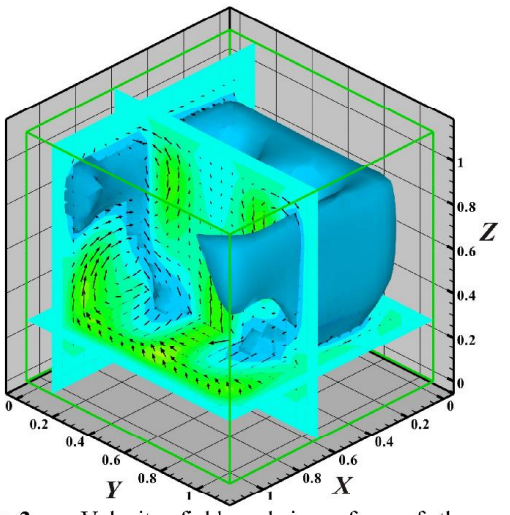

Figure 3 Velocity field and isosurface of the vertical velocity component at $Ra = 10^5$

Temperature isosurfaces and contours at $Br = 1$, $k_{fs} = 0.0037$, $\tau = 100$ and different values of the Rayleigh number are presented in Figure 4 and Figure 5.

The increase in heat source temperature in 10 times is reflected in modification of the temperature field in the gas cavity. Formation of the thermal plume not only in the center of the contaminant source, but also on each side is observed. It is caused by influence of conductive heat transfer in solid walls on natural convection in the gas cavity. Figure 5 shows the decrease in temperature near to the wall $0 \le X \le 0.06$. It is caused by more intensive gas motion.

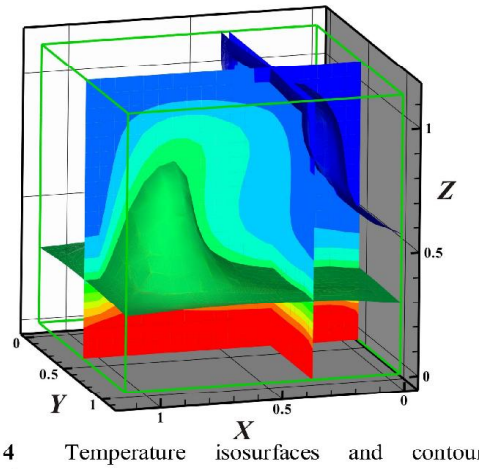

Figure 4 Temperature isosurfaces and contours at $Ra = 10^4$

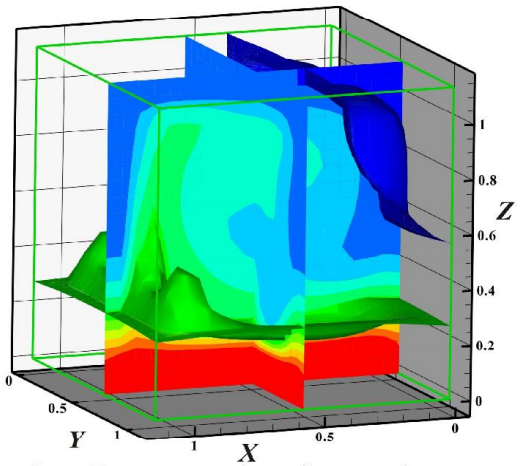

Figure 5 Temperature isosurfaces and contours at $Ra = 10^5$

The analysis of the Rayleigh number effect on the average Nusselt number $Nu = \int_{0.06}^{1.06}\int_{0.06}^{1.06} \left|\frac{\partial \Theta}{\partial Z}\right|_{Z=0.12} dXdY$ at the heat source surface and the average Sherwood number $Sh = \frac{1}{0.35}\int_{0.06}^{1.06}\int_{0.71}^{1.06} \left|\frac{\partial \xi}{\partial Z}\right|_{Z=0.12} dXdY$ at the contaminant source surface has been carried out (Figure 6).

The presented graphic dependences of the average Nusselt and Sherwood numbers as functions of the Rayleigh number and the buoyancy ratio evidently show the typical increase in the heat and mass transfer intensity on the heat source and contaminant source surfaces at the Rayleigh number ranging $10^4 \le Ra \le 10^5$. It should be noted that the buoyancy concentration force $(Br = 1)$ leads to the heat and mass intensification.

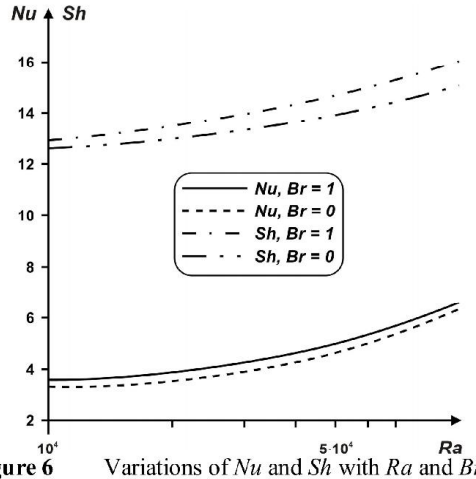

Figure 6 Variations of *Nu* and *Sh* with *Ra* and *Br* at $k_{fs} = 0.0037$, $\tau = 100$

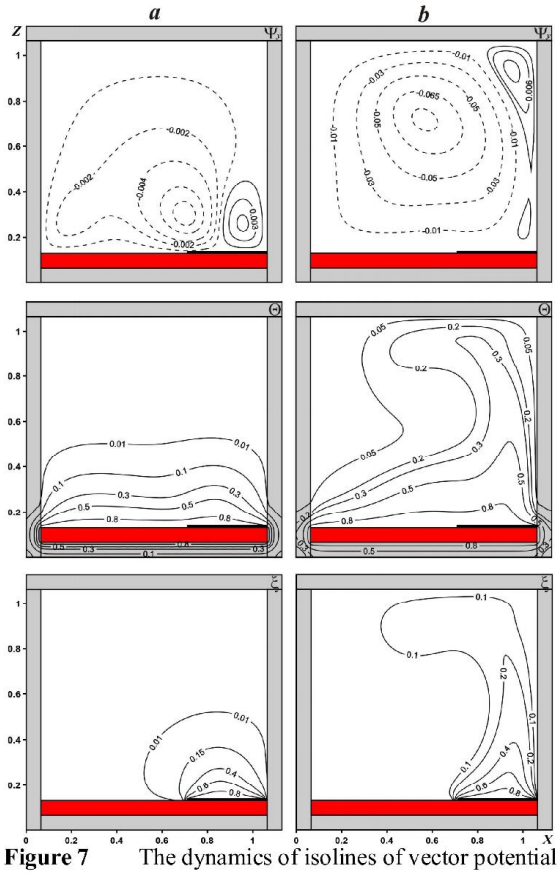

Figure 7 The dynamics of isolines of vector potential function Ψ_y, isotherms Θ and isoconcentrations ξ at: $\tau = 2 - a$, $\tau = 6 - b$

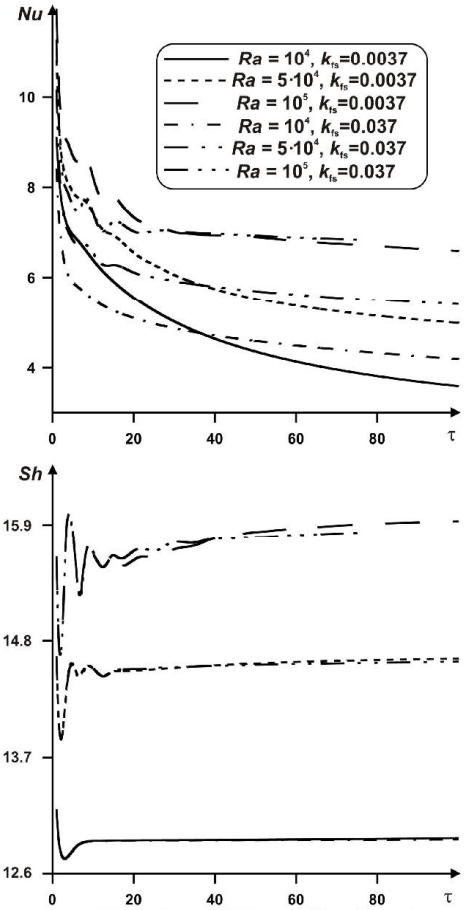

Figure 8 Variations of *Nu* and *Sh* with τ, *Ra* and k_{sf}

The dynamics of the vector potential function Ψ_y formation and temperature fields formation at $Y = 0.56$ for $Ra = 5 \cdot 10^4$, $Br = 1$ are shown in Figure 7.

Figure 7 evidently shows the formation of the convective cells and the temperature field in the gas cavity. It should be noted that the buoyancy concentration force reflects formation of the thermal plume above the contaminant source. The increase in the dimensionless time from $\tau = 2$ up to $\tau = 6$ at $Ra = 5 \cdot 10^4$ leads to the increase in the intensification of the convective flow in the gas cavity $|\Psi_{\max}|_{\tau=2} = 0.01 < |\Psi_{\max}|_{\tau=6} = 0.075$. The latter is reflected in the increase in the sizes of the left vortex which in turn attenuates the intensity of the right convective cell. The temperature field also undergoes changes.

Variations of the average Nusselt and Sherwood numbers with the dimensionless time at different values of the Rayleigh number and the thermal conductivity ratio are shown in Figure 8. Stabilization of the concentration field occurs long before stabilization of the temperature field. The increase in the thermal conductivity ratio leads both to the decrease in the average Nusselt number at $\tau < 40$ and to the increase in the average Nusselt number at $\tau > 40$.

It should be noted that the increase in the thermal conductivity ratio leads to the insignificant changes of the average Sherwood number.

CONCLUSIONS

Mathematical simulation of the double-diffusive conjugate natural convection in the three-dimensional enclosure having finite thickness walls with local heat and contaminant sources in the presence of convective-radiative heat exchange with an environment has been carried out. The distributions of velocity fields, isosurfaces of the vertical velocity component, isolines of vector potential function Ψ_y, temperature and concentration fields in wide range of defining parameters $10^4 \le Ra \le 10^5$, $k_{fs} - 0.037,\ 0.0037$, $Br = 0,\ 1$ have been obtained. The influence of the defining parameters such as the Rayleigh number, the dimensionless time, the buoyancy ratio and the thermal conductivity ratio on formation of heat and mass transfer modes has been analyzed.

ACKNOWLEDGMENTS

This work was performed according to the Russian Federal Purpose Program during 2009-2013 years (No. P 357) and was supported by the Russian Foundation for Basic Research (No. 08-08-00402-a).

REFERENCES

[1] Sezai, I., and Mohamad, A.A., Three-dimensional double-diffusive convection in a porous cubic enclosure due to opposing gradients of temperature and concentration, *Journal of Fluid Mechanics*, Vol. 400, 1999, pp. 333-353.

[2] Mohamad, A.A., and Bennacer, R., Double diffusion, natural convection in an enclosure filled with saturated porous medium subjected to cross gradients; stably stratified fluid, *International Journal of Heat and Mass Transfer*, Vol. 45, 2002, pp. 3725-3740.

[3] Jer-Huan Jang, Wei-Mon Yan, and Hui-Chung Liu, Natural convection heat and mass transfer along a vertical wavy surface, *International Journal of Heat and Mass Transfer*, Vol. 46, 2003, pp. 1075-1083.

[4] Chourasia, M.K., and Goswami, T.K., Three dimensional modeling on airflow, heat and mass transfer in partially impermeable enclosure containing agricultural produce during natural convective cooling, *Energy Conversion and Management*, Vol. 48, 2007, pp. 2136-2149.

[5] Chakraborty, S., and Dutta, P., Three-dimensional double-diffusive convection and macrosegregation during non-equilibrium solidification of binary mixtures, *International Journal of Heat and Mass Transfer*, Vol. 46, 2003, pp. 2115-2134.

[6] Papanicolaou, E., and Belessiotis, V., Double-diffusive natural convection in an asymmetric trapezoidal enclosure: unsteady behavior in the laminar and the turbulent-flow regime, *International Journal of Heat and Mass Transfer*, Vol. 48, 2005, pp. 191-209.

[7] Fu-Yun Zhao, Di Liu, and Guang-Fa Tang, Natural convection in a porous enclosure with a partial heating and salting element, *International Journal of Thermal Sciences*, Vol. 47, 2008, pp. 569-583.

[8] Alloui, Z., Dufau, L., Beji, H., and Vasseur, P., Multiple steady states in a porous enclosure partially heated and fully salted from below, *International Journal of Thermal Sciences*, Vol. 48, 2009, pp. 521-534.

[9] Oosthuizen, P.H., and Paul, J.T., Natural convection in a rectangular enclosure with two heated sections on the lower surface, *International Journal of Heat and Fluid Flow*, Vol. 26, 2005, pp. 587-596.

[10] Kuznetsov, G.V., and Sheremet, M.A., Conjugate natural convection with radiation in an enclosure, *International Journal of Heat and Mass Transfer*, Vol. 52, 2009, pp. 2215-2223.
[11] Kuznetsov, G.V., and Sheremet, M.A., Conjugate natural convection in an enclosure with local heat sources, *International Journal of Computational Thermal Sciences*, Vol. 1, 2009, pp. 341-360.
[12] Samarskii, A.A., Theory of Difference Schemes, *Nauka*, Moscow, 1977.
[13] Bessonov, O.A., Brailovskay, V.A., Nikitin, S.A., and Polezhaev, V.I., Three- dimensional natural convection in a cubical enclosure: a benchmark numerical solution, *Proceedings of the 1st International Symposium on Advances in Computational Heat Transfer*, 1997, pp. 157-165.
[14] Fusegi, T., Hyin, J.M., and Kuwahara, K., A numerical study of 3D natural convection in a differently heated cubical enclosure, *International Journal of Heat and Mass Transfer*, Vol. 34, 1991, pp. 1543-1557.
[15] Kaminski, D.A., and Prakash, C., Conjugate natural convection in a square enclosure effect of conduction on one of the vertical walls, *International Journal of Heat and Mass Transfer*, Vol. 29, 1986, pp. 1979-1988.
[16] Liaqat, A., and Baytas, A.C., Conjugate natural convection in a square enclosure containing volumetric sources, *International Journal of Heat and Mass Transfer*, Vol. 44, 2001, pp. 3273-3280.